PERGAMON

International Journal of Solids and Structures 37 (2000) 6917–6931

INTERNATIONAL JOURNAL OF SOLIDS and STRUCTURES

www.elsevier.com/locate/ijsolstr

Bending and symmetric pinching of pressurized tubes

J.P. Fay [a], C.R. Steele [b,*]

[a] *Department of Aeronautics and Astronautics, Stanford University, Stanford, CA 94305-4035, USA*

[b] *Division of Mechanics and Computation, Department of Mechanical Engineering, Stanford University, Durand Building no. 391, Stanford, CA 94305-4035, USA*

Received 10 November 1999

Abstract

Two experiments quantified the forces necessary for large deformation of an inflated cylindrical tube made of a material with a high elastic modulus. In the first experiment, the end force required to maintain a buckled cylinder at a given kink angle was determined. In the second experiment, the lateral force required to pinch the membrane symmetrically between two flat blades was measured.

An approximate theory is used, based on the observation that during deformation the membrane conserves its initial zero Gaussian curvature in regions free of wrinkling. The novel feature is a simple approximation for the cross-sectional shape. This permits the volume of the deformed cylinder to be quickly calculated. For walls that have negligible extensional and bending energy, the potential energy consists of only the pressure multiplied by the volume and the work of the prescribed load. Minimization of this potential energy yields results for the indentation and buckling problems that are in reasonable agreement with the experimental measurements. For small displacements in the blade pinching experiment, the volume approximation overestimates the force. It is found that a local solution analogous to the Hertzian contact problem provides a better approximation. For the kinked tube with end loading, an interesting feature is a decrease in the load when the fold from one side contacts the opposite side of the tube. The calculations indicate that a minimum potential energy exists with the fold straight. For slightly larger kink angles, however, the fold buckles out of the plane of symmetry. The moment at the single kink, due to the end loads, remains between bounds from the analysis of a pressurized elastic tube with nonpositive stresses. © 2000 Published by Elsevier Science Ltd.

Keywords: Pressure; Tubes; Bending; Pinching

1. Introduction

Nonlinear membrane behavior may be divided into problems in which the modulus of the membrane is either low or high. A low modulus material is typified by a rubber balloon, for which both the nonlinear elastic behavior of the wall and the geometric nonlinearity is important. This problem, with restricted geometric configuration, has been the subject of many papers, as discussed by Jenkins (1991) and Libai and Simmonds (1998). In the present study, we are concerned with a high modulus material, typified by a party

* Corresponding author.

0020-7683/00/$ - see front matter © 2000 Published by Elsevier Science Ltd.
PII: S0020-7683(99)00320-0

balloon made of Mylar, for which the wall is essentially linearly elastic, but the geometric difficulties of unfolding and wrinkling are considerable. Work on this problem is ongoing in several laboratories, such as reported by Liu and Jenkins (1998) and Greschik and Mikulas (1998). Serving as a motivation are the large space structures being planned, with general structural considerations surveyed by Szyszkowski and Glockner (1990), and specific current plans outlined by Lou and Feria (1998). Because accuracy and reliability are desired and ground based simulations are often not possible, numerical simulation of deployment is important. To simplify such simulations, an approximate theory is proposed by Fay and Steele (1999) for the static analysis of joint forces and moments. A potential energy function is used in which the work of the pressure is included, but the strain energy of the wall in extension and bending is generally neglected. The novel feature is the procedure for computing the tube volume. This theory is found to give reasonable agreement with experimental results for the torque in a constrained rolled tube and for asymmetric pinching of a tube by a rigid blade. The application of the torque results in the dynamic process of tube unrolling is given by Steele and Fay (1998).

In the present work, we consider two problems that are more basic and perhaps provide a better examination of the procedure. The first is the symmetric pinching of an inflated tube, which is perhaps the simplest problem involving a large displacement and rigid constraint. The second is the bending of an inflated tube. The perturbation from the initially straight configuration was apparently first considered by Stein and Hedgepeth (1961) and subsequently by Lukasiewicz and Glockner (1984), who report measurements, and by Haseganu and Steigmann (1994), who consider nonlinear material behavior. The pressurized tube has an end moment $M_w = p\pi R_0^3/2$ at which compression (wrinkles) first occur. In this equation, R_0 is the tube radius and p is the internal pressure. With increasing moments, the wrinkled region grows larger, until at $2M_w$, the wrinkles extend around the entire circumference of the tube. We are, however, interested in a post-buckling configuration with a single region of larger deformation, i.e., kinking of the tube. This is significant in the unfolding of an initially flat tube in the "z-fold" configuration.

2. Experiments

Both experiments were performed with a cylinder made from a sheet of urethane covered fabric of thickness $t = 0.25$ mm. When inflated, the urethane formed a cylindrical tube that had a radius $R_0 = 30$ mm and a length $L = 1.380$ m. The ends were plugged with thick PVC caps of the same diameter as the cylinder. An inflation hose passes from a pressure regulator through one of the PVC end caps. A high pressure tank attached to the pressure regulator was used to inflate and maintain the tube at the desired pressure.

2.1. Symmetric blade load

A schematic of the experiment is shown in Fig. 1(a). The membrane was in a wooden cradle that supports both ends. The ends of the tube could not be supported in a manner that allowed them to move towards each other freely, but the end constraint was minimized as much as possible. The device shown in Fig. 2, was used to pinch symmetrically the middle of the membrane with two flat blades. By tightening or loosening the adjustment nuts, the deflection δ could be changed, while at the same time, the stretching of the springs could be monitored so that the pinching force Q could be determined. Thus, the load–deflection curves could be measured for several different values of internal pressure. The resulting data are shown in Fig. 3. Expressed in terms of the dimensionless load and displacement factors, the measurements show little sensitivity to the specific magnitude of pressure. This means that the elastic properties of the wall have little effect on the results and that the wall is behaving almost inextensionally.

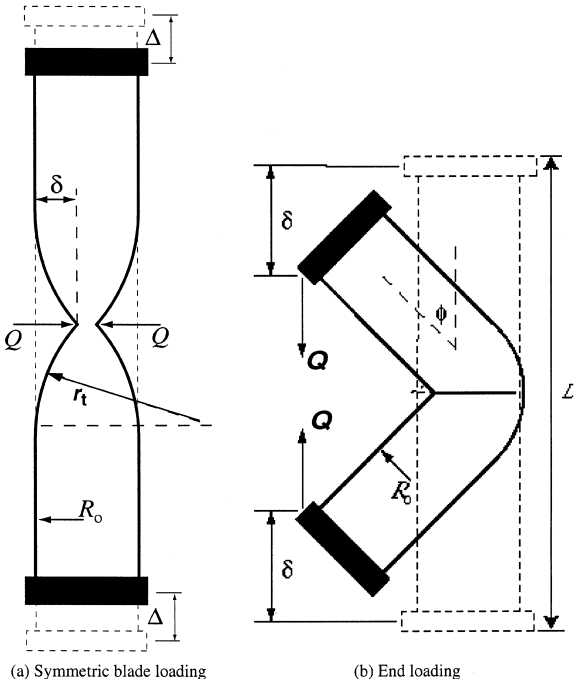

Fig. 1. Schematic of experimental configuration with tube of radius R_0 and Length L. (a) Symmetric blade loading, with the total force Q on each blade and the blade displacement δ. The radius in the region of reversed curvature is r_t. (b) End loading, with end force Q axial displacement δ, and deformed tube angle ϕ.

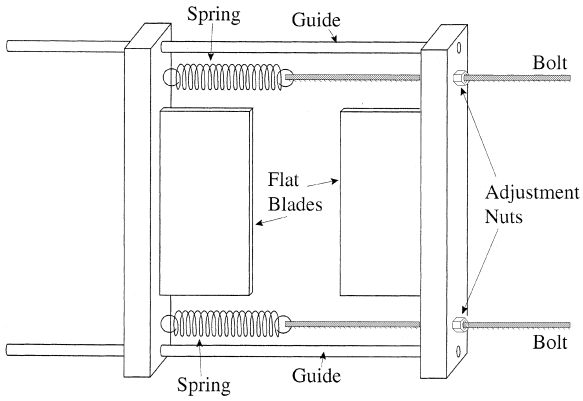

Fig. 2. Symmetric blade measurement and loading device.

2.2. Bending

A schematic of the experiment for tube bending is shown in Fig. 1(b). The urethane tube was hung in the air by its connection to the inflation tube. A chain in series with a calibrated spring connected the two PVC plugs at either end of the tube. By varying the length of the chain, we could alter the angle ϕ of the tube. At each angle, the extension of the spring measured the force Q for a variety of internal pressures. The

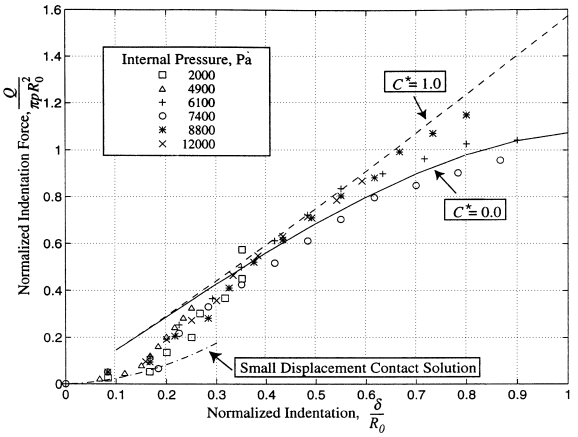

Fig. 3. Symmetric blade results from calculations and experiment.

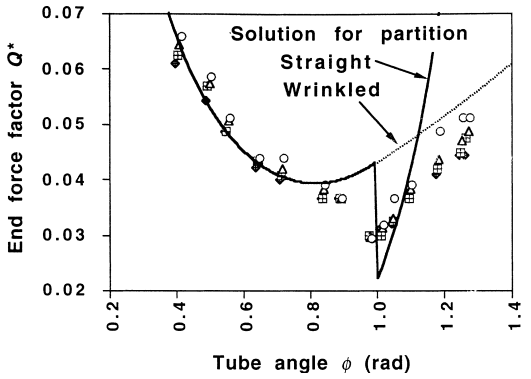

Fig. 4. Relation of load factor $Q^* = Q/(p\pi R^2)$ and angle ϕ for bending of an inflated tube. The force Q and the angle ϕ were measured in the experiment. The points give the measured values for internal pressures (Pa) of 4905 (circles), 6900 (triangles), 8800 (squares), and 11 000 (rotated squares). When the angle is greater than 1 radian, the partition in the center of the fold contacts the lower side of the tube. The volume potential energy solution is shown for the assumptions that the partition remains straight and wrinkled. (Tube urethane, $L = 1.38$ m, $R_0 = 30$ mm, $t = 0.25$ mm.)

resulting data are shown in Fig. 4. Unlike the pinch load tests, a small but systematic dependence on the exact value of pressure can be seen. The lower the pressure, the higher the value of Q^*. In the region where $\phi > 1$, this dependence is more pronounced.

Also of interest is the relation between the load and displacement. The displacement was not measured directly, but an approximation can be computed in terms of the angle. The end displacement factor δ^* is

$$\delta^* = 2\frac{\delta}{L} = 1 - \cos\phi + 4\frac{R_0}{L}\phi\cos\phi. \tag{1}$$

Using this result gives the representation in Fig. 5. Also of interest is the bending of the tube under a pure moment loading of the ends. From the end force test shown in Fig. 1(b), the effective moment at the kink region is approximated by

$$M^* = \frac{2M}{p\pi R^3} = \frac{M}{M_w} = Q^*\left[\frac{L}{R_0}\sin\phi - 4\phi\sin\phi + 2\cos\phi\right]. \tag{2}$$

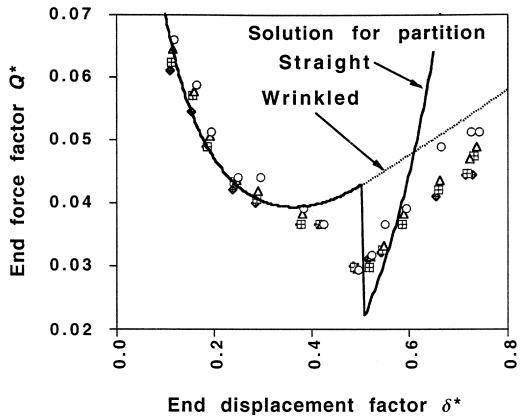

Fig. 5. Same information as shown in Fig. 4, but showing the relation of end force factor Q^* and end displacement factor $\delta^* = 2\delta/L$ for bending experiment. The end displacement for the experimental points is calculated from the angle ϕ using Eq. (1).

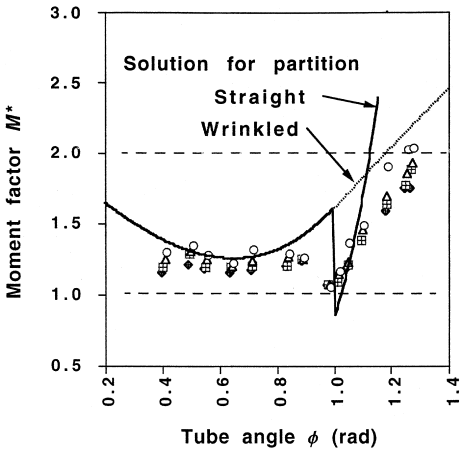

Fig. 6. Same information as in Fig. 4, but showing the relation of end moment factor $M^* = M/(p\pi R^3)$ and rotation angle ϕ. The experimental values for the moment are calculated from the force and the angle in Fig. 4 using Eq. (2). The solution is for the tube with pure bending moment, for which compression of the straight tube occurs at the moment $M^* = 1$ and total collapse should occur at $M^* = 2$.

Using this result gives the representation in Fig. 6. The values of moment for this large deformation lie in the range of $1 < M^* < 2$, which are the limits for wrinkling from the analysis for pure moment loading of Stein and Hedgepeth (1961). Surprisingly, the values of M^* are not too much above 1 for much of the range and reach 2 for the largest deformation measured. For the end force loading, however, the moment is maximum only at the kink region, and the amount of tube material in the region increases with the angle; therefore, a value of 2 may be possible. Of interest is the drop in moment as the angle ϕ equals 1 in Fig. 4. At this angle, the partition formed by the top generator of the tube touches the bottom generator, so for larger angles, the geometry of the kink changes substantially. At sufficiently large angles, $\phi > 1$, the partition is observed to buckle out of the plane of symmetry, to one side or the other, avoiding contact with the lower generator.

3. Approximate theory

The main assumption is that all the work done by the applied loads goes into changing the volume and not into stretching and bending the wall of the tube. Generally, this is valid for a high modulus material with a sufficiently high internal pressure, but not for a rubber balloon. Such an approximation was used by Lukasiewicz and Glockner (1984) for the analysis of a tube with an axial load such as in Fig. 1(b), but with one end rigidly supported and the loaded end is a hemispherical membrane. In the present work, the loaded end is simplified, as a better approximation for the kinked region is proposed, and larger amplitudes of the kink angle are considered, that are significant in the deployment of a z-folded tube. Although some dependence on pressure is evident in the end load results (Fig. 4), which indicates an effect of the wall elastic properties, only the wall with an inextensional reference surface will be considered presently. Consequently, the total potential energy consists of only the work of the internal pressure and the external loads

$$\Pi = -pV - Q\delta - M\phi \tag{3}$$

in which V is the volume of the tube. The difficulty is in determining the volume when a substantial kink is in the tube, and there is contact between different portions of the wall that is not known a priori. However, the task can be accomplished by applying the principles used in Fay and Steele (1999).

3.1. Basic principles for geometry

The principles for the determination of the geometry of the deformed tube are

1. An inextensional surface of zero Gaussian curvature must remain a surface of zero Gaussian curvature in a region of biaxial tension. Thus, the initially flat surface can have a curvature in one direction or the other, but not both, in a region of biaxial tension.
2. In a region of wrinkling, an "averaged" surface may be defined, for which the Gaussian curvature can be either positive or negative. This occurs in a region with a nonpositive component of principal stress.
3. For local equilibrium, constant pressure loading will be carried by constant curvature.
4. Discontinuity in slope occurs only when an external line load is present.

3.2. Deformed tube configuration

The foregoing principles provide an interpretation of the deformed configuration in the two experiments shown in Fig. 1. The pinch load (Fig. 1a) causes local deformation. The "top" (on the left in Fig. 1(a)) and "bottom" (on the right in Fig. 1a) surfaces are in a biaxial tension and by principle (1), they must remain surfaces of zero Gaussian curvature. Consequently, there is a transition from a nonzero component of curvature in the circumferential direction in the main portion of the tube to a nonzero component in the plane of the figure in the deformed region near the load. By principle (3), the radius of curvature is constant in this region with the value r_t. By principle (4), the slope of the top and bottom generators of the cylindrical surface must be continuous except at the concentrated external load. Details of the geometry are shown in Fig. 7. The coordinates x, y are at the beginning of the deformed region, while the angle β is the total angle subtended by the deformed region, and θ is the angle from the edge of the deformed region to the general point P on the top generator. The point S is the point on the bottom generator that has the same arc length along the generator to the tube end as point P. For the pinch load (Fig. 7), the top and bottom generators are symmetric.

For the end loading of the tube shown in Fig. 1(b), the bottom generator can only have the constant curvature in the kink region, while the top generator must fold and form a partition on the plane of

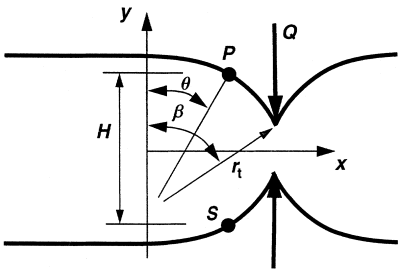

Fig. 7. Geometry for symmetric pinch load. The region near the load Q has the constant radius of curvature r_t and subtends the angle β. The points P and S are equidistant from the tube end and the distance H apart.

symmetry, as also observed by Lukasiewicz and Glockner (1984). For values of the kink angle, $\phi < 1$, the partition extends only partially across the distance to the bottom generator, as indicated in Fig. 8(a). The radius of the bottom generator must be $r_b = 2R_0$. The points P and S remain equidistant from the tube end, so point P must be on the partition. At the angle, $\phi = 1$, the partition contacts the bottom generator. Fig. 8(b) shows one possibility, that the partition remains straight and provides a force on the bottom generator, which therefore can have a slope discontinuity. The radius of the bottom generator is then $r_b > 2R_0$, and the angle subtended is $\beta < \phi$. Another possibility, shown in Fig. 8(c), is that the partition cannot sustain the compressive stress and wrinkles as required in Fig. 8(b). A simple approximation is that all wrinkling occurs at the point of contact with the bottom generator as indicated in Fig. 8(c). As observed in the experiments, the partition actually displaces to one side asymmetrically. However, the approximation (Fig. 8(c)), simulates this as the partition does not interfere with the bottom generator and cause a slope discontinuity.

The cross-section for each of the three cases shown in Fig. 8 is also shown in Fig. 9. The initial inflated tube with the circular cross-section with radius R_0 becomes flattened with the height H, the distance between points P and S. The distance g is the width of the region of the reversed curvature. The membrane must carry the pressure load by curvature in one direction or the other. Therefore, by principle (3), the sides must have a constant radius of curvature. By principle (4), there cannot be a slope discontinuity, so the radius of the sides must be $H/2$. As observed, the sides will wrinkle in the axial direction and form a surface of negative Gaussian curvature. Thus, the sides carry the pressure load by stress in the x^2 direction in Fig. 9, while the top and bottom regions carry the pressure by stress in the direction of the generators. As observed, the plane of the semicircular arcs in Fig. 9, rotates slightly to be normal to the wrinkled surface.

The width of the flat is

$$g = \pi\left(R_0 - \frac{H}{2}\right), \tag{4}$$

and the cross-sectional area is

$$A_{\text{section}} = \pi\left(R_0^2 - \left(R_0 - \frac{H}{2}\right)^2\right). \tag{5}$$

Therefore, from the geometry of the generators, such as in Fig. 7, the coordinates of points P and S can be obtained. Then, the distance H between P and S provides the cross-sectional area.

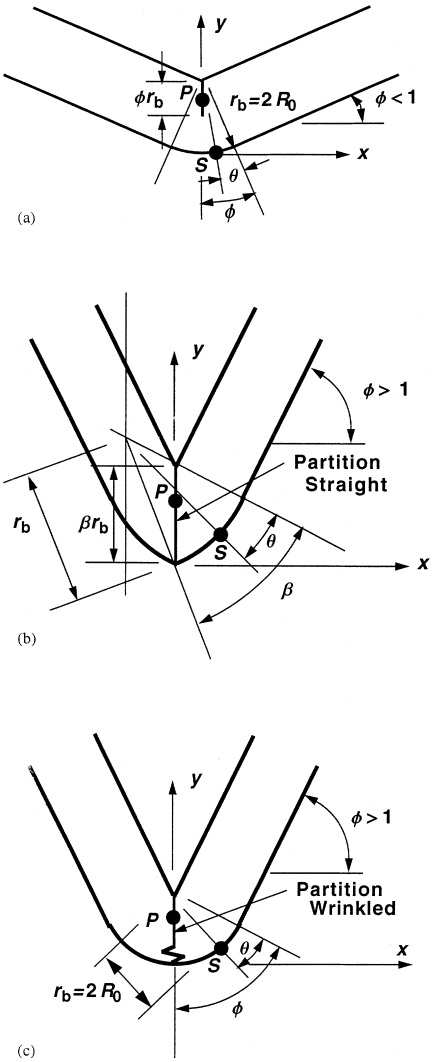

Fig. 8. Geometry for the bending calculations. The surface is inextensional. Therefore in the kinked region the following approximations are used. (a) For $\phi \leqslant 1$, the radius of the lower generator must equal the tube diameter $r_b = 2R_0$, while the upper generator folds and forms a straight partition with the length ϕr_b. (b) For $\phi > 1$, the partition remains straight, but the contact forces a slope discontinuity in the lower generator; so the radius of the lower generator is $r_b > 2R_0$, and the angle is $\beta < \phi$. (c) For $\phi \leqslant 1$, the partition wrinkles at the region of contact with the lower generator, so the radius and the angle of the lower generator are ϕ and $r_b = 2R_0$, as in (a). In all three cases the general points on the lower and upper generators are indicated by Q and S which are at the same arc length from the tube end. Point S is defined in terms of the angle θ.

3.3. Volume integral

We begin with a general form of a volume integral in an arbitrary coordinate system. For the position vector $\mathbf{r} = \mathbf{r}(x^i)$, and base vectors $\mathbf{g}_i = \mathbf{r}_{,i}$, the volume is

$$V = \int\int\int J\,\mathrm{d}x_1\mathrm{d}x_2\mathrm{d}x_3, \tag{6}$$

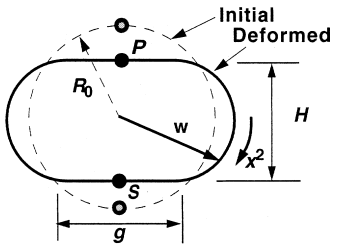

Fig. 9. Cross section of tube on the plane through points P and S which are the distance H apart. The condition that the arc length remains unchanged provides the width of the reverse curvature region g and the area in terms of H and the original radius R_0. The vector $\mathbf{w}$ is from the center to a point on the perimeter, around which the arc length is x^2.

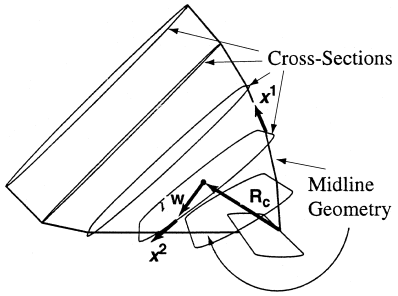

Fig. 10. Three-dimensional wire frame of geometrical approximation. The vector $\mathbf{R}_c(x^1)$ is the position vector from a fixed point to the center of the cross section, and the vector $\mathbf{w}(x^1, x^2)$ is from the center to a point on the perimeter of the cross section.

$$J = \mathbf{g}_1 \cdot (\mathbf{g}_2 \times \mathbf{g}_3). \tag{7}$$

For the present purpose, it is convenient to write the position vector to any point within the space enclosed by the membrane as the sum of a vector to the center point of the cross-section $\mathbf{R}_c$ and a vector in the cross-section $\mathbf{w}$, as indicated in Fig. 10

$$\mathbf{r}(x^1, x^2, x^3) = \mathbf{R}_c(x^1) + x^3\mathbf{w}(x^1, x^2), \tag{8}$$

where x^1 is the parameter of the center line, x^2 is the parameter around the perimeter of the cross-section, that can be taken as the arc length ($0 \leqslant x^2 \leqslant 2\pi R_0$), and x^3 is the fraction distance from the center to the perimeter of the cross-section ($0 \leqslant x^3 \leqslant 1$). Then, Eq. (8) used in Eq. (6) gives

$$\oint \int_0^1 J \, \mathrm{d}x^3 \, \mathrm{d}x^2 = \tfrac{1}{2}\mathbf{R}_{c,1} \cdot \oint (\mathbf{w}_{,2} \times \mathbf{w}) \, \mathrm{d}x^2 + \tfrac{1}{3} \oint \mathbf{w}_{,1} \cdot (\mathbf{w}_{,2} \times \mathbf{w}) \, \mathrm{d}x^2, \tag{9}$$

the first term of which gives the area of the cross-section. The second term is zero for a symmetric cross-section, for which $\mathbf{w}(x^1, x^2 + \pi R_0) = -\mathbf{w}(x^1, x^2)$. This leaves:

$$V = \int \mathbf{R}_{c,1} \cdot \mathbf{n} A_{\text{section}} \, \mathrm{d}x^1 \tag{10}$$

in which A_{section} is the area of the cross-section (Eq. (5)), and $\mathbf{n}$ is the unit normal to the cross-section. The coordinates of points P and S provide all that is needed for the calculation of the volume from Eq. (10). Using from 50 to 500 points in a numerical integration procedure produces essentially the same results.

4. Symmetric blade loading

4.1. Large displacement

For the configuration of the symmetric blade loading of the tube (Fig. 1a), the computation simplifies greatly. The geometry is shown in Fig. 7. Because of the symmetry, the points at the top and bottom of the tube remain at the same axial distance. Thus, the cross-sectional area in the deformed region at the angle θ is

$$A_{\text{section}} = \pi\left[R_0^2 - r_t^2(1-\cos\theta)^2\right]. \tag{11}$$

Therefore, the change in volume from Eq. (10) is

$$\Delta V = -\pi r_t^3 \int_0^\beta (1-\cos\theta)^2 \cos\theta \, d\theta - \pi R_0^2 r_t(\beta - \sin\beta), \tag{12}$$

and the displacement under the load and the axial displacement are

$$\delta = r_t(1-\cos\beta), \tag{13}$$

$$\Delta = r_t(\beta - \sin\beta). \tag{14}$$

An end stiffness C is added to the potential energy (3), and the result can be written in a dimensionless form,

$$\Pi^*(\delta^*, \beta) = \delta^{*^3} F_1(\beta) + \delta^* F_2(\beta) + \tfrac{1}{2} C^* \delta^{*^2} F_2^2(\beta) - Q^* \delta^* \tag{15}$$

in which

$$F_1(\beta) = \frac{\int_0^\beta (1-\cos\theta)^2(\cos\theta)\, d\theta}{(1-\cos\beta)^3}, \tag{16}$$

$$F_2(\beta) = \frac{\beta - \sin\beta}{1-\cos\beta}, \tag{17}$$

and the dimensionless end stiffness is

$$C^* = \frac{C}{p\pi R_0}. \tag{18}$$

The condition for a stationary value of the potential energy provides the relations

$$\frac{\partial}{\partial\beta}\Pi^* = \delta^{*^3} F_1' + \delta^* F_2' + \frac{1}{2} C^* \delta^{*^2} 2F_2 F_2' = 0, \tag{19}$$

$$\frac{\partial}{\partial\delta^*}\Pi^* = 3\delta^{*^2} + F_2 + C^* \delta^* F_2^2 - Q^* = 0. \tag{20}$$

Thus, the problem reduces to a closed form calculation. For a given value of the angle β, the quadratic equation (19) for the displacement δ^* can be solved, and the result substituted into Eq. (20) for the load Q^*. The results for $C^* = 0$ and $C^* = 1$ are shown in Fig. 3. For the larger values of indentation, the agreement with the experimental results is reasonable. For the range of pressures used, the measurements collapse to a single curve with some scatter. The scatter is highest for the larger displacements. However, there is no clear trend with the magnitude of pressure. Therefore, it appears that the small end constraint is somewhat

different in each test and not related to the pressure. If the ends were fixed, then the stiffness C is determined by the axial elastic stiffness of the tube, so that

$$C^* = \frac{8Et}{pL}, \tag{21}$$

for which the pressures used have a value from 120 to 720. Such values used in Eqs. (19) and (20) produce a large increase in the end force for the larger indentation magnitudes, which are off scale in Fig. 3. It is clear that the axial constraint in the experiments was relatively small.

Note that an approximation for the solution can be obtained by taking the first term in the power series expansion for F_1 and F_2 in Eqs. (16) and (17) with the result

$$\beta \approx \left(\frac{6}{5}\right)^{1/2} \delta^*, \tag{22}$$

$$Q^* \approx \frac{4}{3}\left(\frac{6}{5}\right)^{1/2} \delta^* = 1.46\,\delta^*, \tag{23}$$

which gives a straight line in Fig. 3 close to the curve for $C^* = 1$.

For a small indentation, however, the results from Eqs. (19) and (20) give a higher value for the load than the experiments. It is clear that the potential energy with the simple volume approximation captures the main behavior for large displacement, but misses the significant effect for small displacements. An alternate local solution for the small displacement is given in the next section.

4.2. Small displacement–Hertzian contact

For small magnitudes of displacement, the inflated tube can be treated as a flat membrane with the equation,

$$N_x w_{,xx} + N_y w_{,yy} = 0 \tag{24}$$

in which w is the displacement in the normal direction and the prestress in the x- and y-directions are given by the resultants N_x and N_y. For loading along the line where $y = 0$, extending from the point $-a$ to the point $+a$, the solution may be written in terms of a line source.

$$w(x,z) = \int_{-a}^{a} q(\xi)\,\log\sqrt{(x-\xi)^2 + z^2}\,\mathrm{d}\xi, \tag{25}$$

where $z = y\sqrt{N_x/N_y}$, and $q(\xi)$ is the source distribution. The total force acting is

$$Q = 2N_y \lim_{y\to 0} \int_{-a}^{a} \frac{\partial w}{\partial y}\,\mathrm{d}\xi = 2\pi\sqrt{N_x N_y} \int_{-a}^{a} q(\xi)\,\mathrm{d}\xi. \tag{26}$$

The slope along the loaded line is

$$\frac{\partial w}{\partial x}(x,z) = \int_{-a}^{a} q(\xi)\frac{x-\xi}{(x-\xi)^2 + z^2}\,\mathrm{d}\xi, \tag{27}$$

for which the limit with $z = 0$, becomes

$$\frac{\partial w}{\partial x}(x,0) = \int_{-a}^{a} q(\xi)\frac{1}{x-\xi}\,\mathrm{d}\xi. \tag{28}$$

The form of Eqs. (26) and (28) is the same as in the Hertzian contact problem in elasticity. Following Barber (1992), we change the variables to

$$x = a\cos\phi, \quad \xi = a\cos\theta. \tag{29}$$

The integral becomes

$$\frac{\partial w}{\partial x}(x,0) = \int_0^{\pi} q(\theta)\frac{\sin\theta}{\cos\phi - \cos\theta}\,\mathrm{d}\theta, \tag{30}$$

and the force distribution can be written as a Fourier series

$$q(\theta) = \left(\sum_{n=0}^{\infty} q_n \cos n\theta\right) \Big/ (\sin\theta). \tag{31}$$

Only the first term contributes to the resultant force as seen in Eq. (26)

$$Q = 2\pi\sqrt{N_x N_y}\,a\pi q_0. \tag{32}$$

With the result,

$$\int_0^{\pi} \frac{\cos n\theta}{\cos\phi - \cos\theta}\,\mathrm{d}\theta = -\pi\,\frac{\sin n\phi}{\sin\phi}. \tag{33}$$

Eq. (30) becomes

$$\frac{\partial w}{\partial x}(x,0)\,\sin\,\phi = -\pi\sum q_n \sin\,n\phi. \tag{34}$$

For contact between a membrane of curvature R_0 and a straight edge, the local problem is the same as the contact between a flat membrane and a curved edge. Thus, the slope in the contact zone is

$$\frac{\partial w}{\partial x}(x,0)\,\sin\,\phi = \frac{x}{R}\sin\phi = \frac{a}{R}\cos\phi\,\sin\phi = \frac{a}{2R}\sin 2\phi. \tag{35}$$

From Eq. (33), the nonzero coefficients of the load intensity in Eq. (31) are q_0, given by Eq. (32), and q_2

$$q_2 = -\frac{a}{2\pi R}. \tag{36}$$

The condition that the stress is not singular at the ends is

$$q_0 + q_2 = 0, \tag{37}$$

which provides a relation between the load and the width of the contact zone

$$Q = \pi R\sqrt{N_x N_y}\left(\frac{a}{R}\right)^2. \tag{38}$$

Generally, in the contact problem, the magnitude of the displacement cannot be determined from a local consideration because of the logarithmic behavior in Eq. (25). However, for the present problem of two opposed loads on opposite sides of the tube, the condition that the circumference remain unstretched provides the relation between contact distance $2a$ and the displacement δ

$$\delta = \frac{2a}{\pi}. \tag{39}$$

Replacing the contact width in Eq. (38) yields the relation between load and displacement

$$Q = \pi R\sqrt{N_x N_y}\left(\frac{\delta\pi}{2R_0}\right)^2. \tag{40}$$

For the pressure loading of a tube, the membrane stress resultants are

$$N_x = pR_0, \quad N_y = \frac{pR_0}{2}, \tag{41}$$

so the load–displacement relation in Eq. (40) becomes

$$Q^* = \frac{1}{\sqrt{2}}\left(\frac{\pi}{2}\right)^2 \delta^{*^2} = 1.744\,\delta^{*^2}. \tag{42}$$

If the finite width of the blade loading of the tube is taken into consideration, then the total force on the blade is

$$Q^* = \frac{B_{\text{width}}}{R_0}\,\delta^* + \frac{1}{\sqrt{2}}\left(\frac{\pi}{2}\right)^2 \delta^{*^2}. \tag{43}$$

For the experimental configuration, the ratio of the blade width to tube radius is

$$\frac{B_{\text{width}}}{R_0} = 0.067, \tag{44}$$

and Eq. (43) produces the curve in Fig. 3, labeled as the small displacement contact solution. Thus, the experimental results make a transition from the quadratic small displacement solution (43) to the nearly linear large displacement result from Eqs. (19) and (20) at displacements $\delta/R_0 = 0.2$.

5. Tube bending

The geometry for the bending of the tube due to the end loading in Fig. 8 yields the expressions for the coordinates of the point S:

$$x_S = r_b[\cos(\phi - \beta) - \cos(\phi - \theta)], \tag{45}$$

$$y_S = r_b[-\sin(\phi - \beta) + \sin(\phi - \theta)]. \tag{46}$$

The total angle is $\beta = \phi$ for cases Fig. 8a and c, and for the case Fig. 8b:

$$\frac{\sin\beta}{\beta} = \sin\phi. \tag{47}$$

The radius of the bottom generator is

$$r_b = \frac{2R_0\sin\phi}{\sin\phi - \sin(\phi - \beta)}. \tag{48}$$

Thus, all the geometry in Fig. 8 and consequently the volume from Eq. (10) depends only on the value of the tube kink angle ϕ. The displacement of the force at the end is

$$\delta = \frac{L}{2}(1 - \cos\phi) + 2R_0\sin\phi + r_b[-\sin\phi + \sin(\phi - \beta) + \beta\cos\phi]. \tag{49}$$

The potential energy (3), with zero end moment M, gives the result for the load for a given kink angle ϕ

$$Q = -\frac{p\frac{\partial V}{\partial\phi}}{\frac{\partial\delta}{\partial\phi}}. \tag{50}$$

For zero end force Q, the result for the end moment is

$$M = -p\frac{\partial V}{\partial \phi}. \tag{51}$$

Expressions (50) and (51) can be evaluated numerically and provide the curves shown in Figs. 4–6. Most interesting is the sudden drop in the end force at the tube angle, $\phi = 1$. The solution for the straight partition for $\phi > 1$, i.e., the geometry in Fig. 8(b), captures this drop rather well. As ϕ becomes larger, the straight partition result is too stiff, giving a value of end force exceeding that from the solution for the wrinkled partition (Fig. 8(c)). The experimental values are quite close to the results from Fig. 8a for $\phi < 1$, reasonably close to the results from Fig. 8b for ϕ near 1 and somewhat lower than the results from Fig. 8c for larger values of ϕ. Since there is more dependence on the pressure in the latter region, it seems that there is some significant elastic strain occurring. For the highest pressure, however, the measured values are close to the calculated curve for the wrinkled partition.

In Fig. 5, the end force is shown as a function of the end displacement. In this post-buckling region, a relatively small eccentric end force is required for the equilibrium. Fig. 6 shows the relation of moment at the kinked region and the kink angle. The solution curves are directly from Eq. (51). Little difference occurs with the calculation of end force from Eq. (50) and then the moment from Eq. (2).

A much simpler approximation for the volume is used by Lukasiewicz and Glockner (1984), namely, the decrease in volume in the kink region is just one-half of the original. The potential energy for $\phi < 1$ is then for the end load

$$\Pi = p\pi R_0^3\phi - Q\delta \tag{52}$$

with the solution,

$$Q^* = \left[\frac{L}{2R_0}\sin\phi + 2(\cos\phi - \phi\,\sin\phi)\right]^{-1}, \tag{53}$$

which gives values only about 25% higher than those from our present volume calculation procedure plotted in Fig. 4. So starting from the initial straight configuration where $\phi = 0$, with initial values of Q^* near 0.5, as in Lukasiewicz and Glockner (1984), the simpler approximation does well in showing the rapid decrease in the load with kink angle. However, it does not show the increase in the end force for $\phi > 0.8$. Furthermore, for pure moment loading, instead of Eq. (52), the potential energy is just

$$\Pi = p\pi R_0^3\phi - M\phi, \tag{54}$$

which gives the result that the moment to maintain the kink has the value independent of ϕ

$$M^* = 2 \tag{55}$$

rather than the more detailed behavior in Fig. 6 obtained from the present procedure.

6. Conclusions

The large deformation of a tube with internal pressure is a challenging problem. However, in the previous experiments (Fay and Steele, 1999), it was observed that deformation can be characterized in a simple and straight forward manner by considering the basic principles of the behavior of thin shells. This provides an approximation for the volume of the deformed tube, which is needed for the potential energy. Subsequently, little numerical work is needed for theoretical results that are in reasonable agreement with the experiments. In the present study, two configurations that are more basic are solved by the same approach. The conclusion is that the proper level of complexity has been obtained. A more simple approximation for

the volume (Lukasiewicz and Glockner, 1984) misses some important features. More elaborate approximations for the volume involving more degrees of freedom have been found to have a negligible effect.

For the present configurations, the use of load normalized by the pressure force acting on the cross-section enables the experimental values over a substantial range of pressure to collapse to an essentially a single curve. These curves should be valid for a wide variety of materials and geometries.

For the pinch loading, the volume calculation overestimates the force for small amplitudes of displacement. However, a local Hertzian contact solution yields the correct result. The singular behavior at the local contact provided by the Hertzian solution is completely missed by the volume approximation. The main feature is that the force–displacement relation is quadratic for small displacement and almost linear for large, the opposite of the usual situation.

For the end loading, the moment at the kink is rather benign, remaining between the bounds of 1 and 2 for a substantial range of kink angle. However, an intriguing drop in moment occurs at $\phi = 1$, when the fold forms a partition that touches the opposite side of the tube. This is properly described by the volume calculation. The implication is that for a small range of kink angle near $\phi = 1$, the partition is under compression without wrinkling in the minimum potential energy state. The magnitude of the compression is, however, small and the partition is stabilized by a substantial tension in the orthogonal direction. Nevertheless, this seems to violate the often invoked assumption that the thin membrane cannot sustain any compression.

The general conclusion is that the volume calculation, based on the observations and basic principles of shell behavior, does a good job in reducing the large displacement problems under consideration to a trivial computation. This approach does not do everything, as in the small displacement pinch, and must be used with care. However, it seems worthy of consideration for extension to a wider class of large displacement, pressurized shell problems.

References

Barber, J.R., 1992. Elasticity, Kluwer Academic Publishers, Dordrecht.

Fay, J.P., Steele, C.R., 1999. Forces for rolling and asymmetric pinching of pressurized cylindrical tubes. J. Spacecraft Rockets 36 (4),531–537.

Greschik, G., Mikulas, M.M., 1998. Scale model testing of nonlinear phenomena with emphasis on thin film depopulates. Proceedings, Symposium on Deployable Structures: Theory and Applications, Kluwer Academic Publishers, Cambridge.

Haseganu, E.M., Steigmann, D.J., 1994. Theoretical flexural response of a pressurized cylindrical membrane. Int. J. Solids Struct. 31, 27–50.

Jenkins, C.H., 1991. Nonlinear dynamic response of membranes: state of the art-update. Appl. Mech. Rev. 44 (7), S41–S48.

Libai, A., Simmonds, J.G., 1998. The nonlinear theory of elastic shells. Cambridge University Press, Cambridge.

Liu, X., Jenkins, C.H., 1998. Computational issues in the modeling of wrinkling during parachute deployment. Proceedings, Symposium on Deployable Structures: Theory and Applications, Kluwer Academic Publishers, Cambridge.

Lou, M.C., Feria, V.A., 1998. Development of space inflatable/rigidizable structures technology. Proceedings, Symposium on Deployable Structures: Theory and Applications, Kluwer Academic Publishers, Cambridge, MA.

Lukasiewicz, S.A., Glockner, P.G., 1984. Stability of lofty air-supported cylindrical membranes. J. Struct. Mech. 12 (4), 543–555.

Steele, C.R., Fay, J.P., 1998. Inflation of rolled tubes. Proceedings, Symposium on Deployable Structures: Theory and Applications, Kluwer Academic Publishers, Cambridge, MA.

Stein, M., Hedgepeth, J.M., 1961. Analysis of partly wrinkled membranes. NASA TN D-813.

Szyszkowski, W., Glockner, P.G., 1990. The use of membrane structures in space. Int. J. Space Struct. 5 (2), 106–129.